https://doi.org/10.1016/j.istruc.2024.106349

Influence of compression arrangements on the structural behaviour of concrete filled steel tubes

Jiongyi ZHU[1], Shaoxiang Zhong[1], Lei ZHANG[1], Junbo CHEN[2*] and Tak-Ming CHAN[3]

[1] Dept. of Civil Eng., School of Mechanics and Engineering Science, Shanghai University, Shanghai, China
[2] School of Civil and Hydraulic Engineering, Huazhong University of Science and Technology, Wuhan, Hubei, China
[3] Dept of Civil and Environ. Eng., The Hong Kong Polytechnic University, Hung Hom, Hong Kong

*Corresponding author: junbochen@hust.edu.cn

Abstract: The confining pressure to concrete in concrete filled steel tube (CFST) is related to the dilation of concrete core and the hoop stress of steel tube. Due to the passive confinement nature, confinement initiates when the lateral expansion of concrete exceeds that of steel tube. Poor confining stress at initial stage allows the initiation of microcracks in concrete and weakens the ultimate strength, especially in CFSTs with high strength concrete. This paper aims to improve the initial confinement by changing the load arrangements and compressive behaviours of CFST columns under different axial load conditions are investigated. In total, forty-four CFST specimens are tested under different arrangements of axial compression, namely CFST, steel tube confined concrete (STCC) and one-side concrete loaded CFST (CLCFST). Test results indicate that the ultimate strength of the columns with high strength concrete is improved but the initial stiffness is reduced when the axial compression is only applied to the concrete core at one end (CLCFST) or two ends of the column (STCC). Finite element (FE) models are subsequently established, and then validated against the test results. The validated FE models are used to carry out a comprehensive parametric study to investigate the axial stress distribution in CFST columns with different load arrangements. It is found that the load introduction between concrete and steel tubes is mainly affected by the diameter-to-thickness ratio of steel tube and the friction

coefficient.

Keywords: Concrete filled steel tube; High strength concrete; Confinement; Cross-section resistance; Finite element analysis; Load introduction.

1. Introduction

Concrete filled steel tubes (CFST) are very efficient structural members against compression as the strength of concrete core is improved by the confinement from steel tube. It has been well recognised that the concrete core in CFST is passively confined, which means the confining pressure is introduced by the lateral expansion of the concrete core. In the case of whole-section-loaded CFSTs, the lateral strain of the steel tube is larger than that of the concrete core due to a higher Poisson's ratio in the elastic stage, thus, the confining pressure in this stage is minimal. The confinement would be improved only when the dilation of concrete surpasses that of steel tube. Candappa et al. [1] indicated that the Poisson's ratio of concrete starts to increase when the axial stress reaches 70% of its cylinder strength for normal strength concrete (i.e. cylinder strength lower than 60 MPa), and the percentage raises to 80% for high strength concrete with cylinder strengths higher than 80 MPa. This behaviour results in poor confinement at the initial stage of loading. Such poor confinement allows the microcracks to initiate in concrete, and leads to a significant impact on the stress-strain relationship and the ultimate strength of concrete. Previous experimental research confirmed that this type of stress path influences the ultimate strength of confined concrete in CFST. This differs from that of actively confined concrete and an FRP confined concrete in which confinement starts instantly when the compression is applied [2-5]. Observations explored that this stress-path effect was more

47 significant in CFSTs infilled with high strength concrete with compressive cylinder strengths
48 over 80 MPa [4, 5]. Existing investigations concluded that the lateral expansion of high strength
49 concrete is less when compared with normal strength concrete [6, 7], resulting in lower
50 confinement from steel tubes.

51 To eliminate this unfavourable stress-path influence, two approaches can be used. The first
52 one is to increase the expansion of concrete core. This approach has been studied by many
53 researchers by adding expansive agents in concrete to increase the initial lateral confining stress
54 in the concrete. Xu et al. [8] increased the expansion of concrete by replacing the ordinary cement
55 with expansive cement, and the results showed the bond stress between concrete and steel tube
56 increased by 1.2 to 3.3 times. Ho et al. [9] tested ten CFST columns with expansive agent, and
57 the results showed that the expansive agent could improve the elastic modulus, yield and
58 maximum strengths of CFST. Another approach is to mitigate the lateral deformation of steel
59 tubes. One solution is to externally confine the steel tube by using steel rings [10] or FRP jacket
60 [11], which can provide significant confinement to further improve the strength and ductility of
61 CFSTs. Another solution is to change the load arrangements to reduce the axial stress in steel
62 tube to mitigate the lateral deformation. Steel tube confined concrete (STCC) is an alternative
63 type of CFST which was first proposed by Tomii [12] to avoid any external axial stress in steel
64 tubes and the concept has been studied by many researchers afterward [13-17]. The basic concept
65 is to disconnect the steel tube from the beam-column connection, while the external compression
66 is only applied to the concrete core. Researchers have found that when high strength concrete is
67 used, STCC is more effective than CFST [18]. Authors' previous research also showed that the
68 initial confinement in high strength STCC is much higher than the counterpart CFST [19]. It

69 could be concluded that changing load conditions effectively improves the initial confinement
70 for CFST columns [20]. The common STCC refers to the CFST column with compression only
71 applied to concrete at both ends of the column (Fig. 1b). And this paper also examines another
72 load condition that disconnects the steel tube from only one end (Fig. 1c), named concrete-loaded
73 concrete filled steel tube (CLCFST). This load condition is normally adopted in bridge piers
74 where the load from girder is transferred to pier by a bearing plate placed on the top of concrete
75 core. The compression arrangement changes the axial stress distribution between the concrete
76 core and the steel tube, and the load could be transferred from each other by interfacial friction.

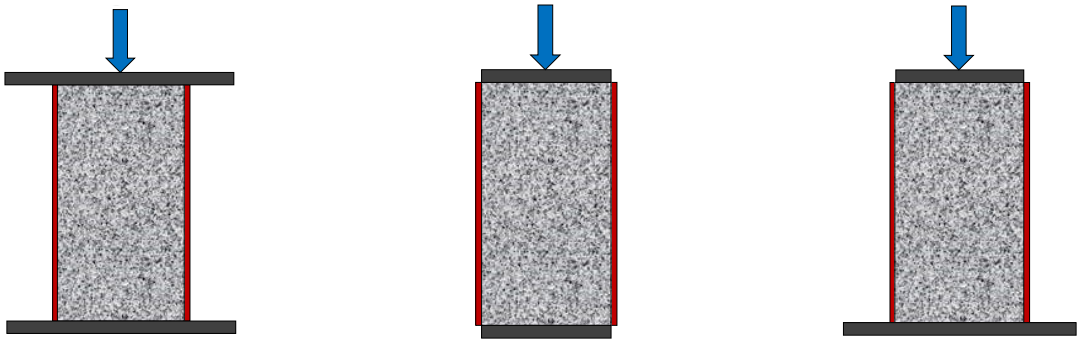

(a) Concrete filled steel tube (b) Steel tube confined concrete (c) One-side loaded CFST

Fig. 1. Loading cases for CFST, STCC and CLCFST

77 To understand the stress distribution and stress path of the STCC and CLCFST column, the
78 column could be separated into two regions in vertical direction, namely load transferring zone
79 and load transferred zone, as shown in Fig. 2. In load transferring zone, the concrete core is
80 bearing most of the applied axial load, and the axial load is introduced to the steel tube by the
81 friction and bonding stress. As the load introduction length increases, the axial force is
82 accumulated in the steel tube until the load is fully transferred. Then the steel tube and concrete
83 bear the axial compression simultaneously, and the load ratios of the concrete and the steel tube
84 in load transferred zone are similar to that in CFST columns. Thus, the load introduction length
85 is crucial to understand the interaction between concrete and steel in STCC and CLCFST, and

the key parameters are the frictional coefficient and confining pressure. Giakoumelis and Lam [21] studied the effect of interfacial condition on the behaviour of CFST. CFST specimens with and without greased interface were tested, and results indicated that the effect of interfacial treatment was insignificant to the load capacity of CFSTs with normal strength concrete. However, the effect was significant when the high strength concrete was used, and a reduction of 17% of load capacity could be observed. A similar conclusion was also drawn by Guler et al. [22], the reduction of load capacity due to loss of interfacial force was also influenced by the D/t ratio and cross-section shapes.

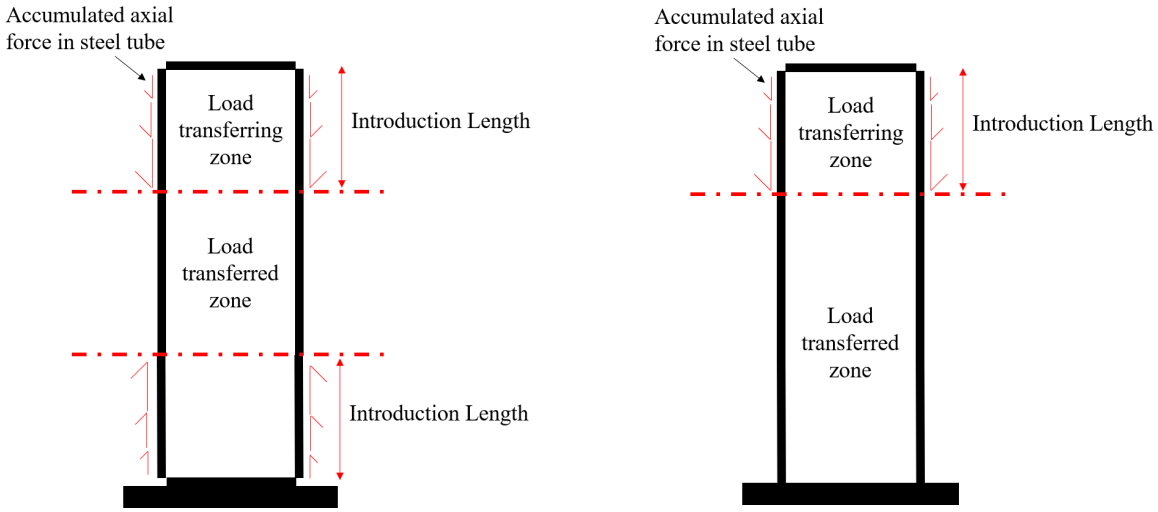

(a) STCC (b) CLCFST

Fig. 2. Classified regions of STCC and CLCFST

Based on the abovementioned research background, the research needs could be summarised as follows:

1. The change of the load arrangements can improve the initial confinement and mitigate the stress-path influence of CFSTs, especially in CFSTs with high strength concrete. The structural behaviours of CFSTs under different load arrangements are worthy to study.
2. The axial load introduction length is the key to understanding the behaviour of STCC and CLCFST. The influence of relevant parameters such as initial bonding strength, interfacial

101 friction, confinement ratio and concrete strength should be studied.

102 Aimed at the abovementioned research needs, this paper presents an experimental
103 investigation of the CFSTs under different load conditions and FE analysis was also conducted
104 to investigate the axial load distribution of those columns.

105 **2. Experimental investigation**

106 **2.1 Specimens**

107 In total, forty-four specimens with circular cross-section were prepared, including forty-two
108 composite specimens and two hollow section counterparts. All the specimens were constructed
109 using commercially available standard S355 hot-finished steel tubes. Two sizes of circular tubes
110 with diameter by thickness of 168.3 mm × 5 mm and 168.3 mm × 6.3 mm were used in this test
111 programme. Nominal cylinder strengths of concrete are 25 MPa, 45 MPa and 80 MPa. To
112 investigate the influence of compression arrangements on the structural behaviour of CFSTs, the
113 specimens were tested under three loading cases, namely whole-section-loaded concrete filled
114 steel tube (CFST), concrete-loaded steel tube confined concrete (STCC) and one-end-concrete-
115 loaded concrete filled steel tube (CLCFST), as shown in Fig. 1. To investigate the effects of
116 initial bonding strength, a series of specimens were heavily greased using oil to reduce the bond
117 between the steel tube and concrete core. The remaining specimens are non-greased and the
118 internal surface of the steel tube was left in an "as-received" condition to model the most likely
119 condition in construction industry for actual columns. The dimensions of all the specimens are
120 listed in Table 1, where D is the external diameter of the circular section, t is the thickness of
121 steel tubes and L is the length of the specimens. The specimens label system is defined as A-B-
122 C-D: A stands for column types where C1 is for CFST, C2 is for STCC and C3 is for CLCFST;

123 B stands for the contact surface treatment (G is for greased surface and N is for “as-received”
124 condition without treatment); C stands for the nominal cylinder strength of concrete; and D
125 indicates the tube thickness.

126 **Table 1.** Details of the specimens.

Load method	Bonding	Designation	D mm	t mm	L mm	f_y MPa	f_c' MPa
CFST	Greased	C1-G-25-5	168.3	5.0	500	373.9	26.8
		C1-G-45-5	168.3	5.0	500	373.9	46.4
		C1-G-80-5	168.3	5.0	500	373.9	84.0
		C1-G-25-6.3	168.3	6.3	500	478.7	26.8
		C1-G-45-6.3	168.3	6.3	500	478.7	46.4
		C1-G-80-6.3	168.3	6.3	500	478.7	84.0
	Non-greased	C1-N-25-5	168.3	5.0	500	373.9	26.8
		C1-N-45-5	168.3	5.0	500	373.9	46.4
		C1-N-80-5	168.3	5.0	500	373.9	84.0
		C1-N-80-5-R	168.3	5.0	500	373.9	84.0
		C1-N-25-6.3	168.3	6.3	500	478.7	26.8
		C1-N-45-6.3	168.3	6.3	500	478.7	46.4
		C1-N-80-6.3	168.3	6.3	500	478.7	84.0
		C1-N-80-6.3-R	168.3	6.3	500	478.7	84.0
STCC	Greased	C2-G-25-5	168.3	5.0	500	373.9	26.8
		C2-G-45-5	168.3	5.0	500	373.9	46.4
		C2-G-80-5	168.3	5.0	500	373.9	84.0
		C2-G-25-6.3	168.3	6.3	500	478.7	26.8
		C2-G-45-6.3	168.3	6.3	500	478.7	46.4
		C2-G-80-6.3	168.3	6.3	500	478.7	84.0
	Non-greased	C2-N-25-5	168.3	5.0	500	373.9	26.8
		C2-N-45-5	168.3	5.0	500	373.9	46.4
		C2-N-80-5	168.3	5.0	500	373.9	84.0
		C2-N-80-5-R	168.3	5.0	500	373.9	84.0
		C2-N-25-6.3	168.3	6.3	500	478.7	26.8
		C2-N-45-6.3	168.3	6.3	500	478.7	46.4
		C2-N-80-6.3	168.3	6.3	500	478.7	84.0
		C2-N-80-6.3-R	168.3	6.3	500	478.7	84.0
CLCFST	Greased	C3-G-25-5	168.3	5.0	500	373.9	26.8
		C3-G-45-5	168.3	5.0	500	373.9	46.4
		C3-G-80-5	168.3	5.0	500	373.9	84.0
		C3-G-25-6.3	168.3	6.3	500	478.7	26.8
		C3-G-45-6.3	168.3	6.3	500	478.7	46.4
		C3-G-80-6.3	168.3	6.3	500	478.7	84.0
	Non-greased	C3-N-25-5	168.3	5.0	500	373.9	26.8
		C3-N-45-5	168.3	5.0	500	373.9	46.4
		C3-N-80-5	168.3	5.0	500	373.9	84.0
		C3-N-80-5-R	168.3	5.0	500	373.9	84.0
		C3-N-25-6.3	168.3	6.3	500	478.7	26.8
		C3-N-45-6.3	168.3	6.3	500	478.7	46.4
		C3-N-80-6.3	168.3	6.3	500	478.7	84.0
		C3-N-80-6.3-R	168.3	6.3	500	478.7	84.0

127 Note: R means repeated tests.

128

129 **2.2 Material properties**

To determine the steel material properties, three tensile coupons were extracted along the longitudinal direction from selected tubes of each size at mid-height. These coupons were tested in accordance with EN ISO 6892-1:2020 [23] with Instron 8803 Fatigue Testing System with a capacity of 500 kN. The basic material properties, namely the elastic modulus (E), yield strength (f_y), ultimate tensile strength (f_u), yield strain (ε_y), strain when strain hardening initiates (ε_{st}), strain corresponding to the ultimate tensile strength (ε_u) and elongation at fracture based on the original gauge length (ε_f), obtained from coupon tests are presented in Table 2.

Table 2. Material properties of steel tubes.

Coupon	E	f_y	ε_y	ε_{st}	f_u	ε_u	ε_f
	GPa	MPa	$\mu\varepsilon$	-	MPa	-	-
5.0 mm	211.1	373.9	1771	2.65%	515.6	18.3%	36.4%
6.3 mm	210.5	478.7	2274	2.40%	554.9	12.8%	34.6%

The concrete used to fill the steel tubes was mixed and cast in the laboratory. The concrete was mixed using ordinary Portland cement, aggregates with a maximum size of 20 mm, sand as fine aggregate, water and superplasticizer (high-range water-reducing admixtures). The concrete mix proportions of the three concrete grades based on saturated surface dry (SSD) condition are listed in Table 3. Nine standard concrete cylinders with a diameter of 150 mm and a height of 300 mm were prepared during the concrete infilling of specimens for each concrete grade. The cylinders were tightly wrapped with cling film and sealed with tape to keep the moisture content and to simulate the curing conditions of the concrete that was infilled in the tubes. The cylinders were tested on the test day to obtain the exact concrete strengths of the test specimens. Four strain gauges with a gauge length of 90 mm were attached to the surface of the standard cylinders at 90-degree to each other to obtain the stress-strain curves and the elastic modulus of concrete.

The concrete cylinders were tested under displacement control at a rate of 0.2 mm/min and the testing procedure complied with EN 12390-3:2020 [24]. The elastic modulus for each concrete cylinder was determined through a linear regression of recorded stress over the average reading of strain gauges between the range of $0.1f_c^{'}$ to $0.33f_c^{'}$. Results from cylinder tests, i.e. the compressive cylinder strengths ($f_c^{'}$), axial strain at ultimate strength (ε_{co}), elastic modulus (E_c) and Poisson's ratio (v) are listed in Table 4.

Table 3. Concrete mix proportions.

Target cylinder strength (MPa)	Water/ cement	Water	Cement	Sand	Aggregate		S.P.*1
					10mm	20mm	
	-	kg/m^3	kg/m^3	kg/m^3	kg/m^3	kg/m^3	kg/m^3
25	0.65	221	340	700	380	760	-
45	0.45	189	420	716	430	645	1.5
80	0.25	125	500	710	436	639	10

Note: *1. S.P. is superplasticizer.

Table 4. Material properties of concretes.

Concrete grade	$f_c^{'}$ MPa	ε_{co} $\mu\varepsilon$	E_c MPa	v -
C25	26.8	2740	20879	0.186
C45	46.4	2830	24942	0.194
C80	84.0	3040	34554	0.194

2.3 Tests arrangement and instrumentation

All compression tests were conducted using an MTS compression machine with an axial capacity of 4600 kN. An example of the test set-up is depicted in Fig. 3. The diameter of the loading plates is 4 mm less than the internal diameter of steel tube. Therefore, in STCC and CLCFST specimens, the axial load can be applied to the concrete only. For STCC the loading plates were placed at both ends of columns, while for CLCFST, only one loading plate was placed on top of the specimens. The arrangement of LVDTs and strain gauges is illustrated in Fig. 3.

168 Three LVDTs were used to record the overall shortening of the concrete core, and strain gauges
169 were used to record the axial strain and lateral strain at the mid-height of the steel tube. For the
170 CLCFST specimens, the axial strain and lateral strain at two additional sections were recorded,
171 as shown in Fig. 3, to investigate the stress distribution in the steel tube.

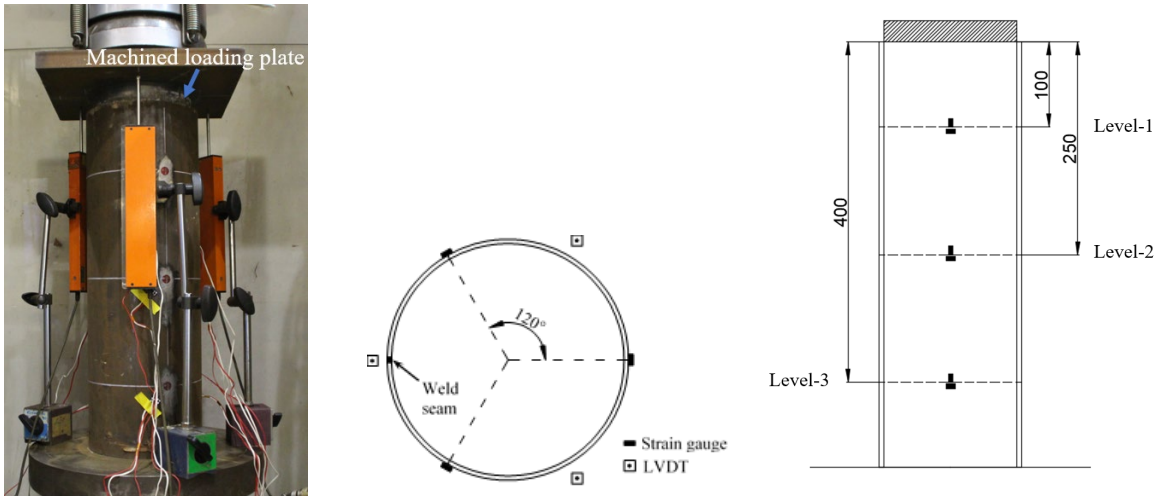

(a) Set-up (b) Arrangement of LVDTs and strain gauges

Fig. 3. Test set-up and instrumentations

172

173 **2.4 Test results**

174 **2.4.1 Load bearing capacity**

175 Table 5 presents the test results of each specimen at ultimate condition, in which N_u is the
176 ultimate load, ε_a and ε_l is the axial strain and lateral strain of the steel tube at mid-height of the
177 column at N_u, and ξ is the confinement ratio defined in Eq. (1),

$$\xi = \frac{A_s f_y}{A_c f_c'} \tag{1}$$

178 where A_s and A_c are the cross-sectional areas of steel tube and concrete core, respectively. For
179 CLCFST columns, axial and lateral strains at three sections in vertical direction are listed in
180 Table 5, and the subscripts 1, 2 and 3 are corresponding positions as shown in Fig. 3. The ratio

of load capacity from test results and the nominal yield capacity f_{cc}/f_c' is used as a strength index to reflect the effectiveness of confinement. The enhanced concrete strength f_{cc} is expressed in Eq. (2),

$$f_{cc} = \frac{N_u - A_s \sigma_{su,a}}{A_c} \tag{2}$$

where $\sigma_{su,a}$ is the axial stress of the steel tube when the peak load of the column is reached. This value is obtained from recorded axial strain and lateral strain of the specimens based on the J_2 flow theory of plasticity as the constitutive model of steel. The f_{cc}/f_c' ratios show that great enhancements in concrete strength were found due to the lateral confinement of steel tube, and the enhancement is up to 4.46. Fig. 4 shows the comparison of the strength index f_{cc}/f_c' among different load arrangements, namely CFST, STCC and CLCFST. It could be found the strength index of STCC and CLCFST is slightly higher than CFST counterparts. This observation is consistent with experimental results from O'shea and Bridge [25] and Zhu and Chan [19]. An interpretation is that in those CFST specimens, when the concrete core and steel tube are loaded simultaneously, the premature brittle failure in high strength concrete happens before the concrete is effectively confined. While in STCC and CLCFST specimens, axial stresses in steel tubes at the initial stage of load are minimal, and the steel tubes are fully used to confine the concrete, significantly improving the strength and ductility of high strength concrete. Fig. 5 shows the load capacity of specimens with (G) and without interfacial oil greasing (N), and the influence of oil greasing on the load capacity of the specimens is insignificant for all three different load conditions, indicating the initial bonding strength has a minor influence on the load capacity. The interfacial friction between steel and concrete will be further investigated in the

following numerical studies.

Table 5. Summary of test results.

Specimens	D/t	N_u kN	f_{cc}/f_c'	ε_a $\mu\varepsilon$	ε_l $\mu\varepsilon$	$\varepsilon_{a\text{-}1}$ $\mu\varepsilon$	$\varepsilon_{l\text{-}1}$ $\mu\varepsilon$	$\varepsilon_{a\text{-}3}$ $\mu\varepsilon$	$\varepsilon_{l\text{-}3}$ $\mu\varepsilon$
C1-G-25-5	33.66	1828	2.81	59346	-53645				
C1-G-45-5	33.66	2009	1.39	24918	-44977				
C1-G-80-5	33.66	2605	1.09	1848	-575				
C1-G-25-6.3	26.71	2595	4.10	46127	-34146				
C1-G-45-6.3	26.71	2929	2.08	38775	-26348				
C1-G-80-6.3	26.71	3482	1.27	6427	-1798				
C1-N-25-5	33.66	1944	2.83	34330	-29552				
C1-N-45-5	33.66	2025	1.16	1746	-7074				
C1-N-80-5	33.66	2731	1.11	1781	-611				
C1-N-80-5-R	33.66	2715	1.01	1895	-503				
C1-N-25-6.3	26.71	2653	3.85	46409	-28438				
C1-N-45-6.3	26.71	2878	2.61	30571	-31436				
C1-N-80-6.3	26.71	3346	1.72	4764	-4090				
C1-N-80-6.3-R	26.71	3300	1.45	5731	-2067				
C2-G-25-5	33.66	1895	3.35	41183	-48886				
C2-G-45-5	33.66	2099	1.43	1784	-922				
C2-G-80-5	33.66	2932	1.37	1672	-4044				
C2-G-25-6.3	26.71	2697	4.46	25468	-67858				
C2-G-45-6.3	26.71	2896	2.48	26072	-23268				
C2-G-80-6.3	26.71	3556	1.56	2984	-1647				
C2-N-25-5	33.66	1885	3.16	57920	-65857				
C2-N-45-5	33.66	2093	1.68	3833	-3018				
C2-N-80-5	33.66	2971	1.30	1726	-841				
C2-N-80-5-R	33.66	2950	1.31	1785	-1017				
C2-N-25-6.3	26.71	2674	4.32	21734	-53344				
C2-N-45-6.3	26.71	2832	2.60	24346	-20566				
C2-N-80-6.3	26.71	3453	1.51	2690	-1379				
C2-N-80-6.3-R	26.71	3647	1.65	2980	-1684				
C3-G-25-5	33.66	1863	3.03	60589	-61646	43308	-55656	18008	-43054
C3-G-45-5	33.66	2130	1.42	5638	-2506	7035	-7752	4899	-3967
C3-G-80-5	33.66	2886	1.19	1751	-755	4535	-1391	1711	-897
C3-G-25-6.3	26.71	2654	4.12	61098	-60176	25055	-31046	52309	-37161
C3-G-45-6.3	26.71	2894	2.73	18320	-27426	9593	-10255	19598	-14744
C3-G-80-6.3	26.71	3505	1.65	2699	-1298	3514	-3798	3761	-2316
C3-N-25-5	33.66	1882	3.06	59245	-61218	42872	-55041	49351	-44067
C3-N-45-5	33.66	2080	1.46	2006	-897	4706	-4530	5316	-2538
C3-N-80-5	33.66	2727	1.16	1628	-711	1804	-7842	1612	-674
C3-N-80-5-R	33.66	2875	1.16	5153	-748	1558	-1352	1865	-2747
C3-N-25-6.3	26.71	2710	4.21	67059	-65900	36348	-46301	52401	-37256
C3-N-45-6.3	26.71	2868	2.63	26681	-23312	17186	-19005	14678	-13363
C3-N-80-6.3	26.71	3583	1.71	4483	-3252	2956	-3219	5987	-4556
C3-N-80-6.3-R	26.71	3496	1.65	3357	-1829	3697	-3515	6227	-5294

Note: R means repeated tests. Compressive strain is taken to be positive.

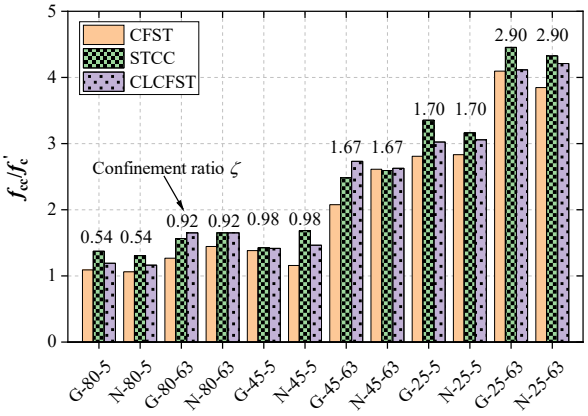

Fig. 4. Comparisons of f_{cc}/f_c' among different load arrangements

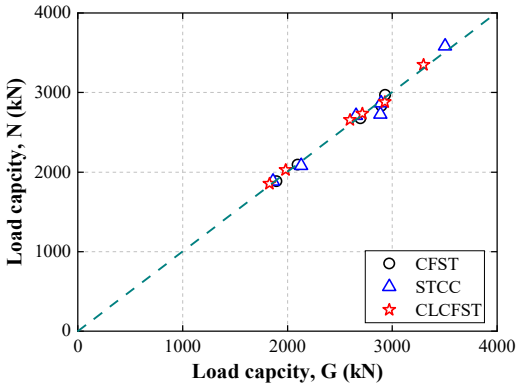

Fig. 5. Influence of interfacial oil greasing on the load capacity of the specimens

2.4.2 Load-shortening responses

Fig. 6 shows the load-shortening responses of all specimens. It could be concluded from the curves that the main difference between specimens under three load conditions is the initial stiffness. The initial stiffnesses of the CFSTs are higher than its STCC and CLCFST counterparts, except for specimen series of C-80-5, which has a very low confinement ratio. The initial slope, defined as the slope between loads ranging from 10% to 33% load capacity, is summarised in Fig. 7. To ensure accurate comparisons, the initial slopes of all specimens are normalized based on the slope of the corresponding whole-section-loaded CFST specimens. It was observed that the initial stiffness of STCC and CLCFST specimens are much lower than the CFST counterparts, and the difference increases as the steel contribution ratio increases. This observation can be attributed to the fact that, in the initial stage, for the specimens of STCC and CLCFST, the concrete predominantly bears the load, with only a minor axial load transferred to the steel tube through interfacial stress, however, in CFSTs the steel tube resisted the axial load directly, and its high Young's modulus improves the initial stiffness significantly. Another observation from Fig. 6 is that the strength and ductility of CFST specimens in the C-80-5 series are not as good

as those STCC and CLCFST, which can be obtained from the post-peak behaviour. The reason could be attributed to the insufficient confinement for the high strength concrete at the initial stage of loading.

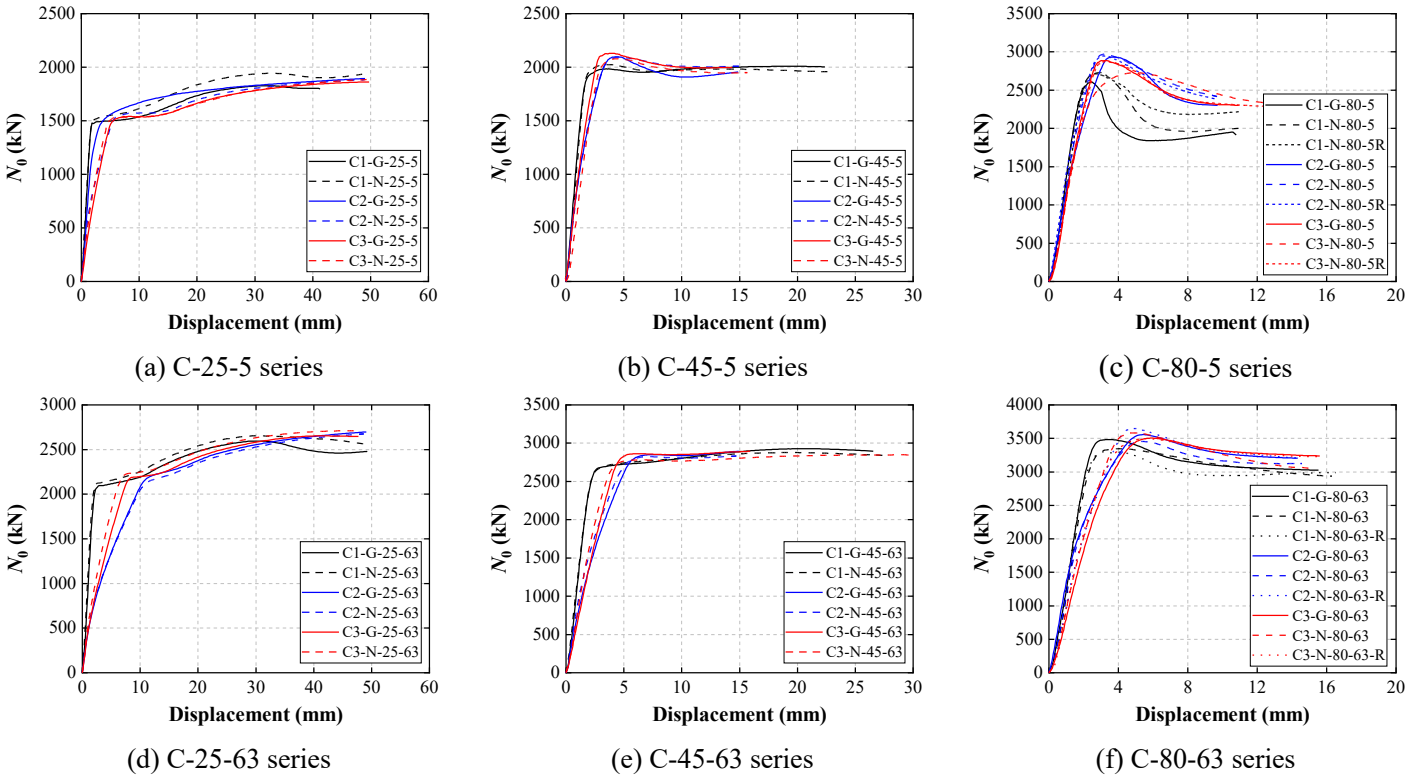

(a) C-25-5 series (b) C-45-5 series (c) C-80-5 series

(d) C-25-63 series (e) C-45-63 series (f) C-80-63 series

Fig. 6. Load-shortening curves of all the specimens

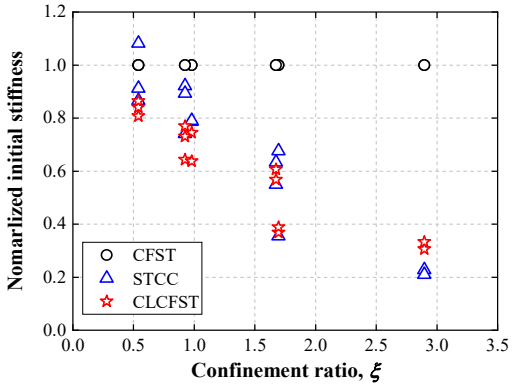

Fig. 7. Relationships of initial stiffness reduction and confinement ratio

3 Finite element modelling

3.1 Finite element models

In this paper, commercial finite element (FE) software ABAQUS [26] was adopted to

227 establish the FE models of CFST, STCC and CLCFST specimens. For the FE modelling of CFST,
228 STCC and CLCFST, four-node shell element, S4R, is selected for the steel tube [27-30], while
229 eight-node solid element, C3D8R, is used for the concrete core [31-33]. The axial displacement
230 is applied at the top of the concrete core and the steel tube for CFST columns, while for STCC
231 and CLCFST specimens the displacement is only imposed on concrete core. The bottom surfaces
232 of CFST and CLCFST columns are constrained in all degrees of freedom, while in these STCC
233 columns only the concrete surface is constrained in all degrees of freedom. The interfacial
234 contact between steel tube and concrete core is modelled. The "Hard" contact provided in
235 ABAQUS, which allows the separation of two surfaces, was adopted. The tangential behaviour
236 between the two surfaces is modelled by the Coulomb friction criteria.
237 Mesh convergence studies were conducted prior to FE modelling. The optimal mesh size
238 was found by comparing the axial load to axial shortening relationship until the curves converged.
239 It is found that the load-shortening curves are almost identical when the mesh size of steel tube
240 and concrete core are $D/35$, $D/30$ and $D/25$, Thus, the adopted mesh sizes of steel tube and
241 concrete core are $D/25$, respectively. In existing literature, the friction coefficient between steel
242 and concrete ranges from 0.25 to 0.75. Friction coefficients of 0.25, 0.3, 0.5, 0.6 and 0.75 were
243 used by Schneider [34], Hassanein et al. [35], Ouyang and Kwan [36], Han et al. [37] and Al
244 Zand et al. [38], respectively. In the current study, calibration of the friction coefficient was
245 conducted using the values 0.25, 0.4, 0.6, and 0.75. For each specimen, FE modelling was
246 performed with these four coefficients, and the FE results were compared to the experimental
247 results. The mean N_{FE}/N_{test} values are 1.12, 0.99, 0.97 and 0.97, respectively. Consequently, a
248 friction coefficient of 0.4 was selected for validating the FE model.

A quad-linear hardening model including a yield plateau, as shown in Fig. 8, was used for steel. In this model, two parameters should be provided, i.e. the strain when strain hardening initiates ε_{st}, and the strain corresponding to the ultimate tensile strength ε_u. Empirical equations proposed by Tao et al. [30], as shown in Eq. (3) and Eq. (4), were used. The slope of the strain hardening phase was taken as $0.02E$.

$$\varepsilon_p = \begin{cases} 15\varepsilon_y & f_y \le 300\,\text{MPa} \\ \left[15 - 0.018\left(f_y - 300\right)\right]\varepsilon_y & 300\,\text{MPa} \le f_y \le 800\,\text{MPa} \end{cases} \tag{3}$$

$$\varepsilon_u = \begin{cases} 100\varepsilon_y & f_y \le 300\,\text{MPa} \\ \left[100 - 0.15\left(f_y - 300\right)\right]\varepsilon_y & 300\,\text{MPa} \le f_y \le 800\,\text{MPa} \end{cases} \tag{4}$$

The concrete damaged plasticity model (CDP) in ABAQUS was adopted to model the nonlinear behaviour of the confined concrete. In this model, a Poison ratio, v, equal to 0.2, and the measured Young's modulus E_c were adopted. The flow potential eccentricity e and the viscosity parameter μ_v were taken as constant values of 0.1 and 0.0001, respectively. The dilation angle ψ was determined by Eq. (5), in which ξ is the confinement ratio. The ratio of the compressive strength under biaxial loading to the uniaxial compressive strength $f_{b0}/f_c^{'}$ was calculated from Eq. (6), proposed by Papanikolaou and kappos [39], and the ratio of the second stress invariant on the tensile meridian to that on the compressive meridian K_c was determined using the expression recommended in Tao et al. [30], as given in Eq. (7). The stress-strain model of concrete core inside the steel tube suggested by Tao et al. [30] was used, as shown in Fig. 9.

$$\psi = \begin{cases} 56.3\left(1 - \xi\right) & \text{for } \xi \le 0.5 \\ 6.672e^{\frac{7.4}{4.64+\xi}} & \text{for } \xi > 0.5 \end{cases} \tag{5}$$

$$\frac{f_{b0}}{f_c^{'}} = 1.5\left(f_c^{'}\right)^{-0.075} \tag{6}$$

$$K_c = \frac{5.5}{5 + 2\left(f_c^{'}\right)^{0.075}} \tag{7}$$

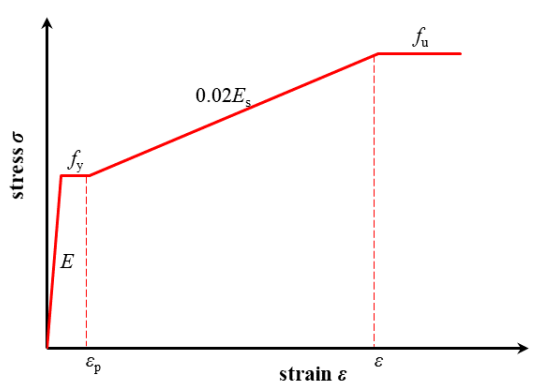

Fig. 8. Constitutive model of steel

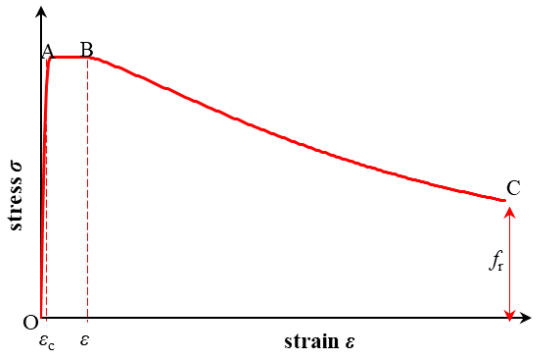

Fig. 9. Constitutive model of concrete

In the experiment, the load-displacement curve of each specimen and the axial strain at 250 mm of CFST and STCC as well as the axial strain at 100 mm, 250 mm and 400 mm of CLCFST from the bottom were recorded. These test results were used to validate the FE models. Figs. 10-12 show the comparisons of load-axial shortening relationships between test and FE results under different loading arrangements. The FE results and the test data were in good agreement except the softening behaviour of the CFST specimens with low confinement ratio (i.e.C1-G-80-5) because the low confinement allows serious shear failure to occur in the concrete core and the current FE model cannot capture this type of failure. Fig. 13 shows the load-axial strain relationships of the CLCFST specimens at different positions along the column height. It could be found the FE model can capture the axial strain distribution along the column height. Fig. 14 illustrates the comparisons of load capacities between FE and experimental results. The average N_{FE}/N_{test} ratios for CFST, STCC, and CLCFST are 0.99, 1.01 and 1.03, respectively, with coefficient of variance (CoV) values of 0.02, 0.02 and 0.03, respectively. These results indicate that the proposed modelling method effectively captures the load capacities of the CFST, STCC and CLCFST specimens. The validated FE models were then used to further analyse the axial stress distribution and the main factors affecting the load transferring and the load introduction

280 length.

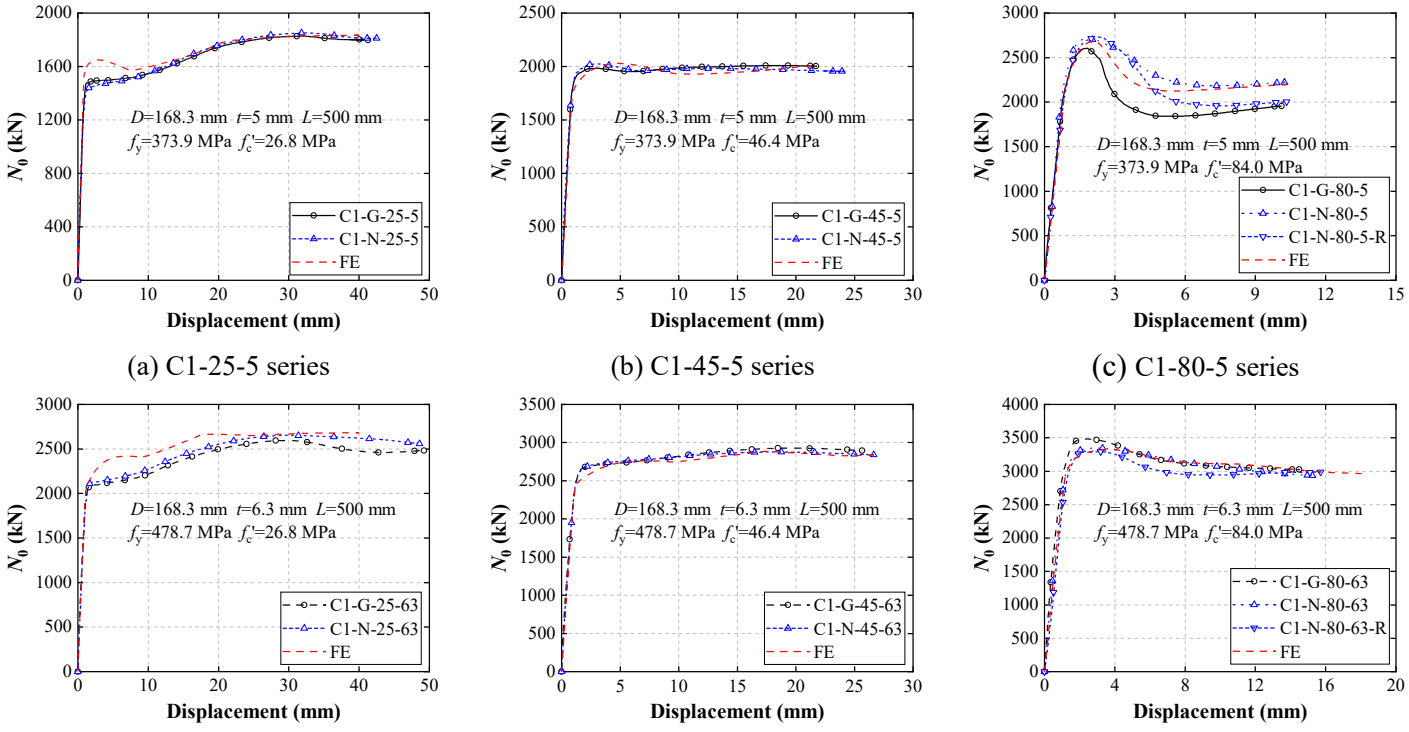

(a) C1-25-5 series (b) C1-45-5 series (c) C1-80-5 series

(d) C1-25-63 series (e) C1-45-63 series (f) C1-80-63 series

Fig. 10. Comparisons of load-displacement curves between CFST specimens and FE models

281

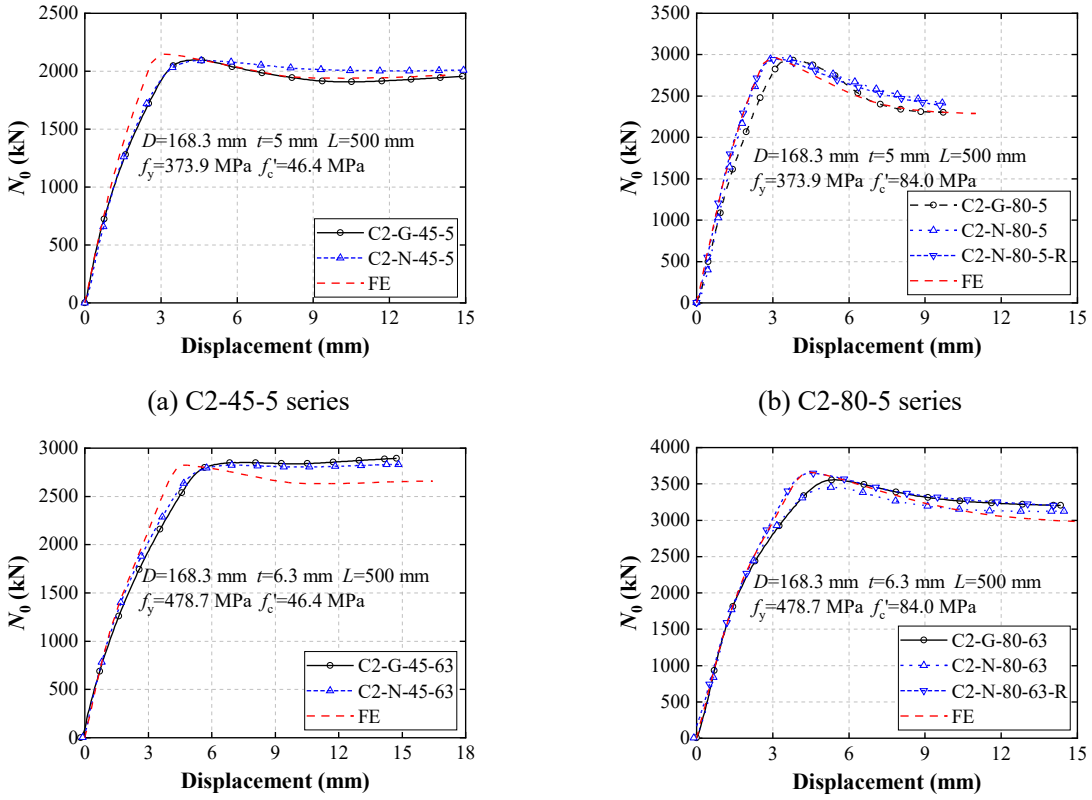

(a) C2-45-5 series (b) C2-80-5 series

(c) C2-45-63 series (d) C2-80-63 series

Fig. 11. Comparisons of load-displacement curves between STCC specimens and FE models

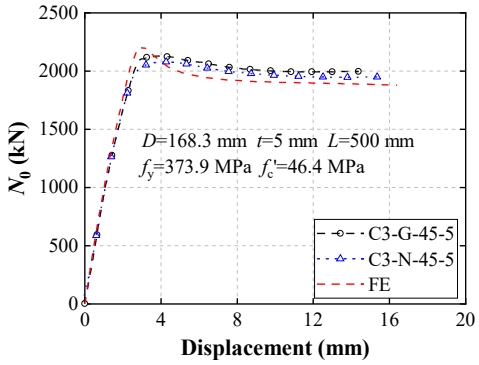

(a) C3-45-5 series

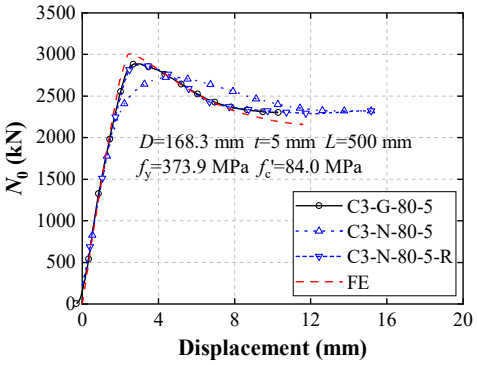

(b) C3-80-5 series

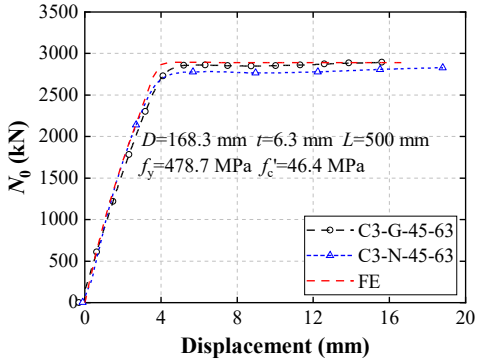

(c) C3-45-63 series

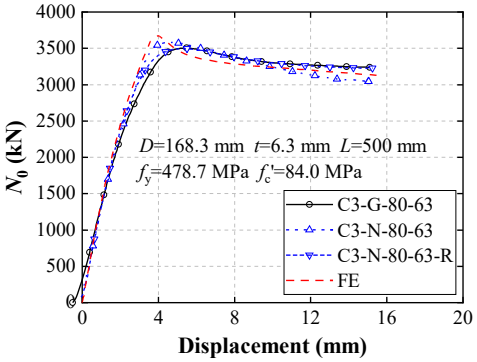

(d) C3-80-63 series

Fig. 12. Comparisons of load-displacement curves between CLCFST specimens and FE models

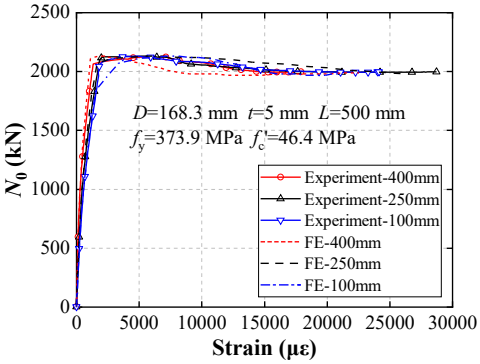

(a) C3-45-5 series

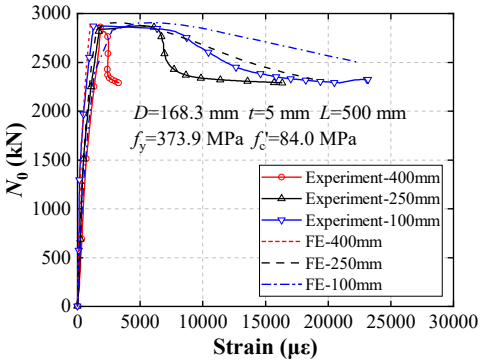

(b) C3-80-5 series

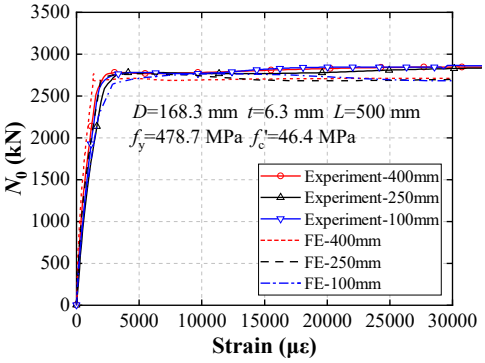

(c) C3-45-63 series

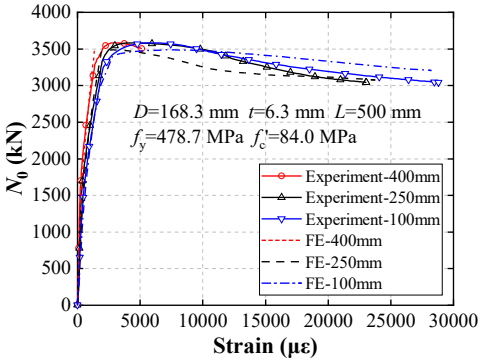

(d) C3-80-63 series

Fig. 13. Comparisons of load-axial strain relationship of test data and FE results.

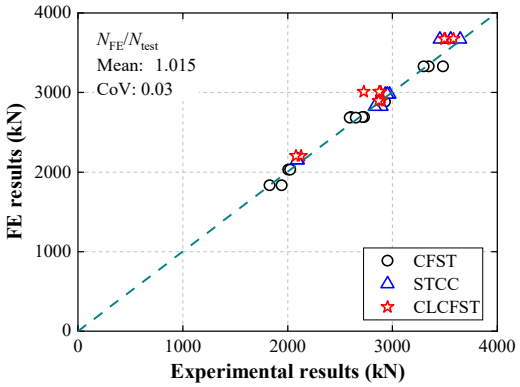

Fig. 14. Comparisons load capacities between FE and experimental results.

3.2 Load introduction length

The above validation indicates that the FE models can successfully replicate the experimental results. To study the axial load distribution ratio between the concrete core and the steel tube. The axial stresses in steel tube along the longitudinal direction were extracted from the FE results. Fig. 15 shows typical axial load distributions between concrete and steel in CFST, STCC and CLCFST at their peak load, where the vertical axis denotes the column height, and the horizontal axis denotes the axial load ratio of steel tube N_s/N_t, where N_s is the axial load taken by steel tube and N_t is the total axial load taken by the whole section. It could be found the load ratio of CFST is almost identical along the column height expect the 100 mm region close to the top and the end of the column where the load ratio is affected by the boundary condition. For CLCFST, at top of the column (i.e. column height of 500 mm) the axial load in the steel tube is zero due to the load arrangement. The axial load in steel tube increases rapidly along the height due to the accumulated friction force transferred from concrete core. After a certain length, the load ratio of CLCFST meets the load ratio of the CFST column, and is identical to that value afterward. This length is defined as the load introduction length within which the axial load in concrete core is transferred to the steel tube. The load ratios within the load introduction lengths

of the STCC columns are close to those of CLCFSTs, and STCC columns have a symmetrical load introduction zone from the bottom because of the load arrangements. Therefore, it is believed the load ratio in the load introduction zone of STCC and CLCFST is almost identical which means the load arrangement at one end of the column have no influence on the load transfer at the other end. Therefore, only the cases of CLCFST are analysed in the following sections. Fig. 16 shows the load introduction length of the CFST and CLCFST specimens, and the length ranges from 150 mm to 300 mm. Parametric studies are then conducted to further examine factors affecting the load introduction length.

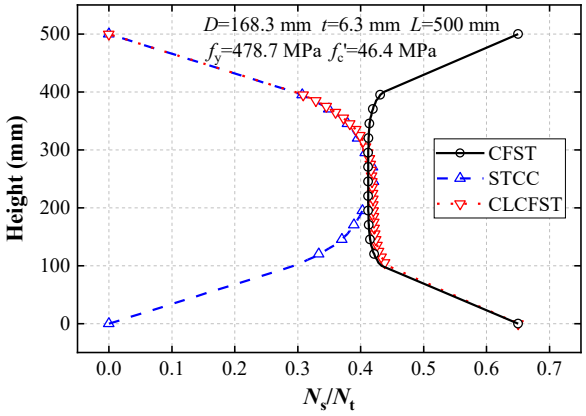

Fig. 15. Typical axial load distributions of CFST, STCC and CLCFST

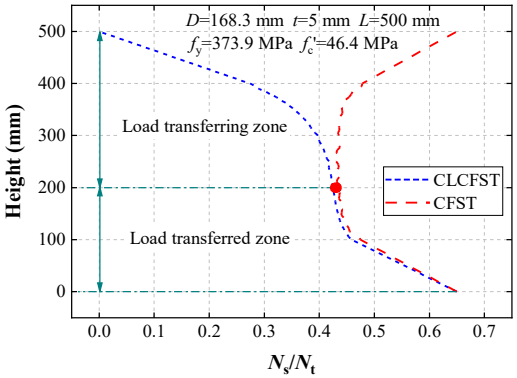

(a) C-45-5

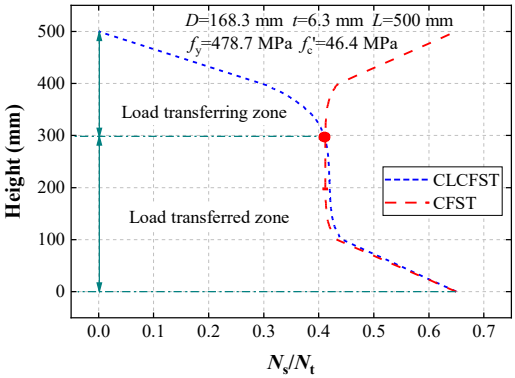

(b) C-45-63

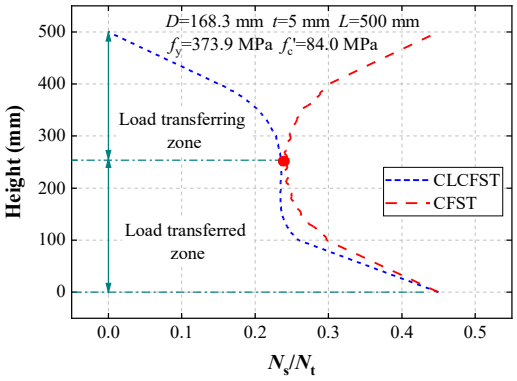

(c) C-80-5

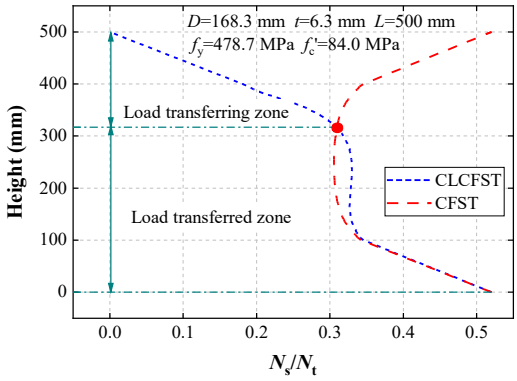

(d) C-80-63

Fig. 16. Comparison of N_s/N_t ratios of CLCFST and CFST specimens

4 Parametric study

The validated FE models were used to carry out a comprehensive parametric study to investigate the influence of diameter-to-thickness ratio (D/t), the yield strength of the steel tube (f_y), the compressive strength of the concrete cylinder (f_c') and the coefficient of friction (μ) on the load introduction length of CLCFST. In the parametric study, the D/t ratio ranges from 10 to 50, f_y ranges from 345 MPa to 580 MPa, f_c' ranges from 40 MPa to 100 MPa, and μ ranges from 0.3 to 0.6.

4.1 Diameter-to-thickness ratio (D/t)

The load introduction length under different D/t ratios is shown in Fig. 17. It is found that the load introduction length is positively associated with the D/t ratio, indicating that more distance is required to accumulate the friction force when the D/t ratio increases. The conclusion could be explained by the expression of confining pressure as follows:

$$f_l = \frac{2\sigma_l t}{D} \tag{8}$$

$$f = \mu \cdot f_l \tag{9}$$

where σ_l is the lateral stress in steel tube, f is the friction. When the D/t increases, and the interfacial confining pressure decreases, thus, the friction force between the concrete and the

steel tube decreases, resulting in a longer load introduction length. Fig. 18 shows the distribution of hoop stresses in steel tube along the longitudinal direction with different D/t ratios which indicates the difference of the confining stresses in load transferring zone is minor.

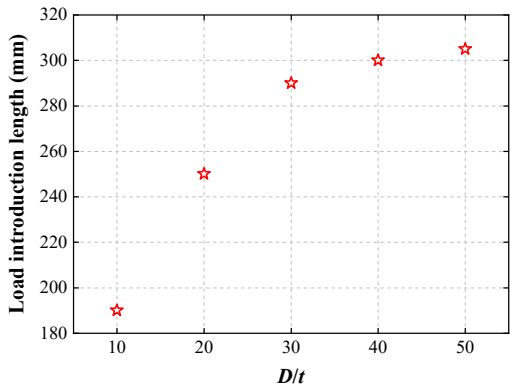

Fig. 17. Load introduction lengths under different D/t ratios

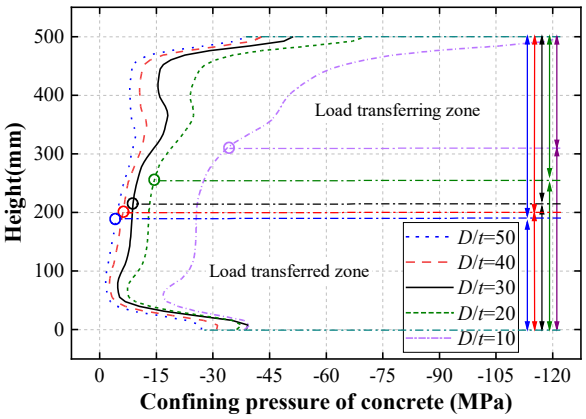

Fig. 18. Distribution of confining pressure in longitudinal direction with different D/t ratio

4.2 Yield strength of the steel tube (f_y)

The influence of the yield strength of the steel, f_y, on the load introduction length is shown in Fig. 19. It is found that steel tubes with different yield strengths have no effect on the load introduction length. The reason also could be explained by Eqs. (8)-(9). It was found that in the FE results most regions in the steel tubes within the load introduction length are still in the elastic stage when the column reaches its peak strength. Thus, the lateral stress in steel tube is only affected by elastic modulus and Poisson's ratio. Therefore, the yield strength (f_y) of the steel tube has no effect on interfacial pressure between steel and concrete.

4.3 Compressive cylinder strength of concrete (f_c')

The influence of the compressive strength of concrete (f_c') on the load introduction length is presented in Fig. 20. It is found that concretes with different cylinder compressive strengths have a minimal effect on the load introduction length. In order to explain this observation, the

confining stress within the load transferring zone is examined, and it is found that the confining stress distribution within the load transferring zone is almost the same when concrete strength changes, thus based on Eqs. (8)-(9), it was concluded that the concrete strength has no influence on the load introduction length.

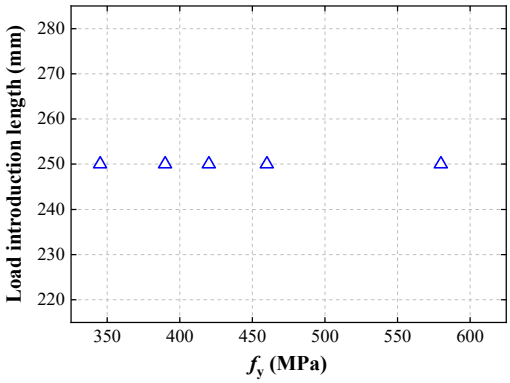

Fig. 19. The load introduction length under different f_y

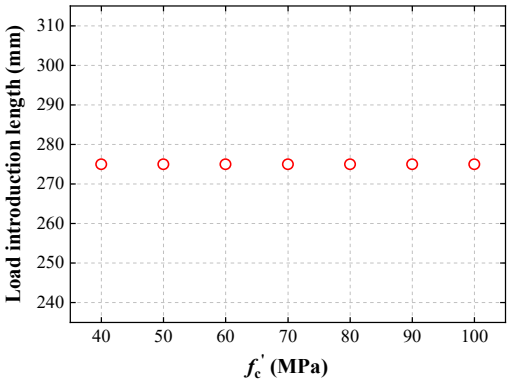

Fig. 20. The load introduction length under different f_c'

4.4 Coefficient of friction (μ)

The effect of the coefficient of friction (μ) on the load introduction length was also investigated. The load introduction lengths with different values of μ are obtained, as shown in Fig. 21. The numerical results show that when the μ value increases from 0.3 to 0.5, the load introduction length decreases significantly, however, when the μ value is larger than 0.5, it has a minor effect on the load introduction length. Fig. 22 shows the distributions of axial load ratio of steel tube along the column height with various of friction coefficients. It could be found when μ is large (e.g. μ=0.6), the transferred load accumulated rapidly first, but the load accumulating rate keeps decreasing. The possible reason is that when the axial load in concrete core decreases, due to the nature of passive confinement, the lateral confining pressure as well as the friction force decrease. Thus, it could be concluded that any attempts to increase coefficient of friction

can enhance the load transfer between concrete core and steel tube but the marginal effect was low when the coefficient larger than 0.6.

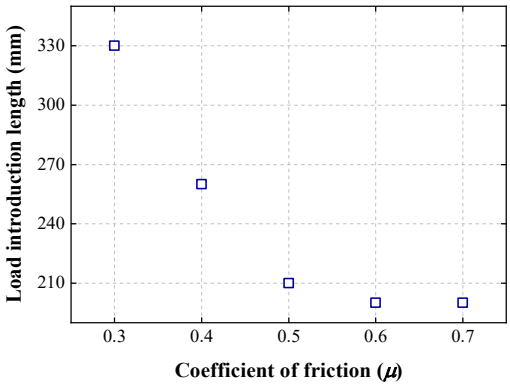

Fig. 21. The load introduction length under different μ

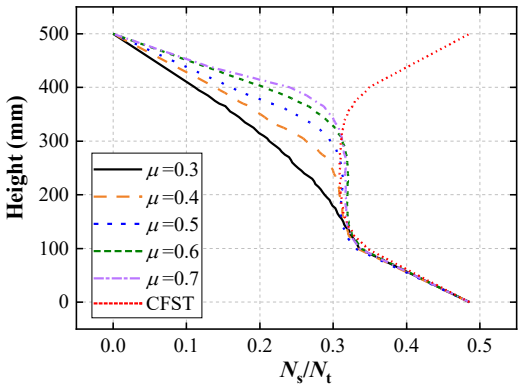

Fig. 22. Distributions of axial load ratio of steel tube with various of friction coefficients

4.5 Summary

In the parametric study, the load transfer between concrete and steel tube in CLCFST and STCC were investigated. It was found diameter-to-thickness ratio and coefficient of friction is the key parameters to the load introduction length of CLCFST and STCC column. Any attempts to increase the confining pressure and coefficient of friction can enhance the load transfer between concrete core and steel tube. The strengths of steel and concrete have no influence on the load introduction length because the material within the load transferring zone is still elastic, and the ultimate strengths of the materials have minimal effects to the confining pressure.

5 Conclusions

This paper presents an experimental investigation on the concrete filled steel tube under three different conditions of compression: CFST, steel tube confined concrete STCC and one-end-concrete-loaded CFST CLCFST. A total of forty-four specimens with circular cross-section were tested under monotonic axial compression. Finite element models were then established

and validated against test results. Based on the validated FE models, a parametric study was conducted. The following conclusions were drawn from experimental and numerical studies in this paper:

1. The changes in compression arrangements from a whole-section-loaded condition to a concrete-loaded condition can improve the effect of confinement at the initial loading stage for CFSTs, especially for those with high strength concrete. The load capacity of STCC and CLCFST is much higher than the CFST counterparts with high strength concrete the increasing percentage is up to 12%. The interfacial oil greasing has a minor influence on the load capacity of concrete under all three different load conditions the average difference is about 0.1%.
2. According to the load-shortening responses, it is found the initial stiffness of the STCC and CLCFST specimens is smaller than that of CFSTs, with an average degradation of approximately 35%. As the confinement ratio increases the difference in initial stiffness becomes larger, with the maximum degradation being about 80% when the confinement ratio reaches 2.9. When high strength concrete is used the strength and ductility (i.e. post-peak softening behaviour) of CFST are not as good as STCC and CLCFST.
3. The diameter-to-thickness ratio (D/t) is an important factor affecting the length of load introduction. The smaller the D/t, the larger the length of load introduction; the reason is that when the D/t decreases, and the interfacial confining pressure becomes larger, thus, the friction force between the concrete and the steel tube increases which results in a shorter load introduction length. The yield strength of the steel tube (f_y) and the compressive strength of the concrete cylinder (f_c') have no effect on the load introduction length. Increasing the

friction coefficient (μ) between the concrete core and the steel tube in STCC and CLCFST can shorten the load introduction length but the improvement becomes minor when the friction coefficient is larger than 0.6.

Acknowledgement

The experimental tests were conducted in the concrete technology laboratory at The Hong Kong Polytechnic University. Assistances from the technical staff on the experimental works and financial support from the Chinese National Engineering Research Centre for steel construction (Hong Kong Branch) are greatly appreciated.

References

[1] Candappa DC, Sanjayan JG, Setunge S. Complete triaxial stress-strain curves of high-strength concrete. Journal of materials in civil engineering. 2001;13:209-15.

[2] Lai MH, Liang YW, Wang Q, Ren FM, Chen MT, Ho JCM. A stress-path dependent stress-strain model for FRP-confined concrete. Engineering Structures. 2020;203:109824.

[3] Lin S, Zhao Y-G, He L. Stress paths of confined concrete in axially loaded circular concrete-filled steel tube stub columns. Engineering Structures. 2018;173:1019-28.

[4] Ho JCM, Lam JYK, Kwan AKH. Effectiveness of adding confinement for ductility improvement of high-strength concrete columns. Engineering Structures. 2010;32:714-25.

[5] Xiao Q, Teng J, Yu T. Behavior and modeling of confined high-strength concrete. Journal of Composites for Construction. 2010;14:249-59.

[6] Jin J, Zhang W, Li F, Li M, Shi Y, Guo Z et al. Robotic binding of rebar based on active perception and

417 planning. Automation in Construction. 2021;132:103939.

418 [7] Ho JCM, Ou XL, Chen MT, Wang Q, Lai MH. A path dependent constitutive model for CFFT column.

419 Engineering Structures. 2020;210:110367.

420 [8] Xu C, Chengkui H, Decheng J, Yuancheng S. Push-out test of pre-stressing concrete filled circular steel

421 tube columns by means of expansive cement. Construction and building materials. 2009;23:491-7.

422 [9] Ho JCM, Ou XL, Li CW, Song W, Wang Q, Lai MH. Uni-axial behaviour of expansive CFST and DSCFST

423 stub columns. Engineering Structures. 2021;237:112193.

424 [10] Lai MH, Ho JCM. Confinement effect of ring-confined concrete-filled-steel-tube columns under uni-axial

425 load. Engineering Structures. 2014;67:123-41.

426 [11] Teng JG, Yu T, Fernando D. Strengthening of steel structures with fiber-reinforced polymer composites.

427 Journal of Constructional Steel Research. 2012;78:131-43.

428 [12] Tomii M. Experimental studies on concrete filled steel tubular stub columns under concentric loading.

429 Proceedings of International Colloquium on Stability of Structures Under Static and Dynamic Loads,

430 SSRC/ASCE/Washington, DC1977.

431 [13] Fam A, Qie FS, Rizkalla S. Concrete-filled steel tubes subjected to axial compression and lateral cyclic

432 loads. Journal of Structural Engineering. 2004;130:631-40.

433 [14] Han LH, Yao GH, Chen ZB, Yu Q. Experimental behaviours of steel tube confined concrete (STCC)

434 columns. Steel and Composite Structures. 2005;5:459-84.

435 [15] Johansson M, Gylltoft K. Mechanical behavior of circular steel-concrete composite stub columns. Journal

436 of Structural Engineering. 2002;128:1073-81.

437 [16] Qi H, Guo L, Liu J, Gan D, Zhang S. Axial load behavior and strength of tubed steel reinforced-concrete

438 (SRC) stub columns. Thin-Walled Structures. 2011;49:1141-50.

[17] Yamamoto T, Kawaguchi J, Morino S. Experimental study of scale effects on the compressive behavior of short concrete-filled steel tube columns. Proceedings of the Conference: Composite Construction in Steel and Concrete IV2000. p. 879-90.

[18] Liu J, Teng Y, Zhang Y, Wang X, Chen YF. Axial stress-strain behavior of high-strength concrete confined by circular thin-walled steel tubes. Construction and Building Materials. 2018;177:366-77.

[19] Zhu JY, Chan TM. Experimental investigation on steel-tube-confined-concrete stub column with different cross-section shapes under uniaxial-compression. Journal of Constructional Steel Research. 2019;162.

[20] Zhu J-Y, Chen J, Chan T-M. Analytical model for circular high strength concrete filled steel tubes under compression. Engineering Structures. 2021;244:112720.

[21] Giakoumelis G, Lam D. Axial capacity of circular concrete-filled tube columns. Journal of Constructional Steel Research. 2004;60:1049-68.

[22] Guler S, Copur A, Aydogan M. A comparative study on square and circular high strength concrete-filled steel tube columns. Advanced Steel Construction. 2014;10:234-47.

[23] UNE-EN-ISO-6892-1. Metallic materials - Tensile testing - Part 1: Method of test at room temperature (ISO 6892-1:2019) is classified in these ICS categories: 77.040.10. 2020.

[24] UNE-EN-12390-3. Testing hardened concrete - Part 3: Compressive strength of test specimens. European Standard. 2020.

[25] O'Shea MD, Bridge RQ. Design of circular thin-walled concrete filled steel tubes. Journal of Structural Engineering. 2000;126:1295-303.

[26] ABAQUS. ABAQUS Standard User's Manual, Vol. 1, 2 and 3. Dassault Systèmes Simulia Crop. 2019;Johnston, RI, USA,Version 2019.

[27] Chan TM, Gardner L. Compressive resistance of hot-rolled elliptical hollow sections. Engineering

461 Structures. 2008;30:522-32.

462 [28] Ellobody E, Young B. Nonlinear analysis of concrete-filled steel SHS and RHS columns. Thin-Walled

463 Structures. 2006;44:919-30.

464 [29] Ma J-L, Chan T-M, Young B. Experimental Investigation on Stub-Column Behavior of Cold-Formed

465 High-Strength Steel Tubular Sections. Journal of Structural Engineering. 2016;142.

466 [30] Tao Z, Wang X-Q, Uy B. Stress-Strain Curves of Structural and Reinforcing Steels after Exposure to

467 Elevated Temperatures. Journal of Materials in Civil Engineering. 2013;25:1306-16.

468 [31] Han L-H. Concrete-Filled Steel Tubular Structures-Theory and Practice. Science Press, Beijing, China

469 (in Chinese). 2007;29:24-.

470 [32] Li W, Han L-H, Chan T-M. Performance of Concrete-Filled Steel Tubes subjected to Eccentric Tension.

471 Journal of Structural Engineering. 2015;141.

472 [33] Sheehan T, Dai XH, Chan TM, Lam D. Structural response of concrete-filled elliptical steel hollow

473 sections under eccentric compression. Engineering Structures. 2012;45:314-23.

474 [34] Schneider SP. Axially loaded concrete-filled steel tubes. Journal of Structural Engineering-Asce.

475 1998;124:1125-38.

476 [35] Hassanein MF, Patel VI, Elchalakani M, Huu-Tai T. Finite element analysis of large diameter high strength

477 octagonal CFST short columns. Thin-Walled Structures. 2018;123:467-82.

478 [36] Ouyang Y, Kwan AKH. Finite element analysis of square concrete-filled steel tube (CFST) columns under

479 axial compressive load. Engineering Structures. 2018;156:443-59.

480 [37] Han L. Concrete Filled Steel Tubular Structures-Theory and Practice (in Chinese). Third. China Science

481 Publishing & Media Ltd; 2016.

482 [38] Al Zand AW, Badaruzzaman WHW, Tawfeeq WM. New empirical methods for predicting flexural

483 capacity and stiffness of CFST beam. Journal of Constructional Steel Research. 2020;164.

484 [39] Papanikolaou VK, Kappos AJ. Confinement-sensitive plasticity constitutive model for concrete in triaxial

485 compression. International Journal of Solids and Structures. 2007;44:7021-48.

486